Nonlinear Analysis: Modelling and Control, Vilnius, IMI, 2001, v. 6, No. 2, 51-69

# Modeling of Pulse Propagation Factor Changes in Type II Second-Harmonic Generation

**A. Kurtinaitis**[a], **A. Dementjev**[b,c], **F. Ivanauskas**[a,d]

[a] Vilnius University, Naugarduko 24, 2600 Vilnius, Lithuania
{andrius.kurtinaitis, feliksas.ivanauskas}@maf.vu.lt
[b] Institute of Physics, Savanorių 231, 2028 Vilnius, Lithuania
aldement@klt.mii.lt
[c] Vilnius University, Saulėtekio al. 9, 2040 Vilnius, Lithuania
[d] Institute of Mathematics and Informatics,
Akademijos 4, 2600 Vilnius, Lithuania

Received: 25.10.2001
Accepted: 02.11.2001

**Abstract**

We describe the simulations of the second harmonic generation of ultrashort laser pulses by numerically solving a system of wave propagation equations. The equations are solved by using a split-step method in two-dimensional cyllindrically symmetric space and time coordinates. The diffraction part of a solution uses the Hopscotch type finite-difference scheme on a regular grid. The transport part is solved by using the cubic spline approximation. The obtained numerical results satisfactorily respect energy conservation constraints.

The algorithm and program developed make it possible to optimize the process of the second harmonics generation and to identify the conditions where sufficiently high degree of the pulse compression with a relatively low degradation of their quality is achieved.

*Keywords:* second harmonics generation, laser pulse compression, finite difference solution, numerical simulation.

## 1 Introduction

The second harmonics generation (SHG) was the first nonlinear optical effect discovered soon after invention of the ruby laser [1]. Huge amount of works has been devoted to various aspects of the SHG. During the last decade, great attention is paid to the compression

dynamics of the second harmonics pulses during the second-type interaction, taking into account the differences of the group velocities of the pulses [2–10]. However, the compression process of both the second- [2–10] and the third-harmonics [11, 12] is usually analysed in the plane-wave approximation. This approach makes it impossible to examine the quality alteration of the interacting pulses [13–17] during the SHG process. Only in recent works by Zhang et al. [18, 19], much attention was paid to the effects related to the transverse structure of the pulses. However, the problem of the quality of the generated pulses, which is very important for practical applications, has not been treated even in these works. Besides, the corresponding equations in the above-mentioned works were solved by using the fast Fourier transform (see also [20, 21]). In the present work, another method for numerical solution of the nonlinear equations of SHG, based on the Hopscotch splitting method and cubic spline approximation, is proposed. This approach can be of interest also when modeling other processes of nonlinear optics [22, 23]. The algorithm and program developed make it possible to perform a detailed modeling of the changes of the spatio-temporal pulse structure during the SHG process in the intense energy interchange regime taking into account the diffraction and the temporal delay of the pulses. The algorithm and program developed thus enable us to carry out the optimization of the SHG process and to find the conditions where the sufficiently high degree of pulse compression is achieved with a relatively low degradation of their quality.

## 2 Theoretical model of type II SHG

The derivation of the shortened equations for the light pulse propagation in the crystals with quadratic nonlinearity, based on the first principles of the nonlinear optics, is presented in [1, 22–26]. Selecting the electrical field of the interacting pulses in the form

$$\begin{aligned}\mathbf{E}(r,z,t) = \mathrm{Re}\,\{&\hat{\mathbf{e}}_1 E_1(r,z,t)\exp\left(ik_1 z - i\omega_1 t\right) + \\ &\hat{\mathbf{e}}_2 E_2(r,z,t)\exp\left(ik_2 z - i\omega_2 t\right) + \hat{\mathbf{e}}_3 E_3(r,z,t)\exp\left(ik_3 z - i\omega_3 t\right)\}\end{aligned} \tag{1}$$

and assuming that the carrier frequencies satisfy the condition of the SHG $\omega_3 = \omega_1 + \omega_2$ ($\omega_1 = \omega_2$), the following set of truncated equations for the second-type interaction $oe - e$ can be readily derived neglecting

walk-off effect for the sufficiently wide axially symmetric beams [18, 23, 25]:

$$\frac{\partial E_1}{\partial z}+\frac{1}{\nu_1}\frac{\partial E_1}{\partial t}-\frac{i}{2k_1}\Delta_r E_1+i\frac{g_1}{2}\frac{\partial^2 E_1}{\partial t^2}+\frac{\alpha_1}{2}E_1=i\sigma_1^{(II)}E_2^*E_3\exp\left(i\Delta kz\right), \quad (2)$$

$$\frac{\partial E_2}{\partial z}+\frac{1}{\nu_2}\frac{\partial E_2}{\partial t}-\frac{i}{2k_2}\Delta_r E_2+i\frac{g_2}{2}\frac{\partial^2 E_2}{\partial t^2}+\frac{\alpha_2}{2}E_2=i\sigma_2^{(II)}E_1^*E_3\exp\left(i\Delta kz\right), \quad (3)$$

$$\frac{\partial E_3}{\partial z}+\frac{1}{\nu_3}\frac{\partial E_3}{\partial t}-\frac{i}{2k_3}\Delta_r E_3+i\frac{g_3}{2}\frac{\partial^2 E_3}{\partial t^2}+\frac{\alpha_3}{2}E_3=i\sigma_3^{(II)}E_1E_2\exp\left(-i\Delta kz\right). \quad (4)$$

Here, the unit vectors of polarization satisfy the conditions $\hat{\mathbf{e}}_1 \perp \hat{\mathbf{e}}_2$, $\hat{\mathbf{e}}_1 \perp \hat{\mathbf{e}}_3$, $\hat{\mathbf{e}}_2 \parallel \hat{\mathbf{e}}_3$, $k_l = n_l\omega_l/c$ are the wave numbers, $n_l$ are the refraction indices, $\nu_l = (dk_l/d\omega)^{-1}$ are the group velocities, $\Delta_r = \partial^2/\partial r^2 + \partial/r\partial r$ is the Laplace operator governing diffraction in the transverse plane, $g_l = d^2k_l/d\omega^2$ are the group-velocity dispersion coefficients, $\alpha_l$ are the absorption coefficients, $\sigma_j^{(II)} = (4\pi\omega_j/cn_j)\, d_{\text{eff}}^{(II)}$ are the nonlinear coupling coefficients, whilst the maximum value of the effective interaction coefficient is $\max d_{\text{eff}}^{(II)} = d_{36}\sin 2\theta_S^{II}$ ($\theta_S^{II}$ is the phase-matching angle), and $\Delta k = k_3 - k_1 - k_2$ is the wave-vector mismatch.

Let us define a few physical quantities that are necessary to discuss the conversion efficiency and quality changes of interacting pulses. First of all, we introduce the intensity of pulses

$I_l(r,t,z) = cn_l|E_l(r,t,z)|^2/8\pi$.

Then the instantaneous power of pulses is defined as

$P_l(t,z) = 2\pi\int\limits_0^\infty I(r,t,z)r\,dr$.

The energy density of the pulses and the total energy of the pulses are defined as $H_l(r,z) = \int\limits_{-\infty}^{\infty} I_l(r,t,z)dt$ and $W_l(z) = \int\limits_{-\infty}^{\infty} P_l(t,z)\,dt$, respectively. The intensity and energy density of the pulses are changing in the free space due to diffraction, but it is well known that the energy of a pulse slice $dW_l = P_l(t)\,dt$ and the energy of the whole pulse do not change due to propagation in free space in the paraxial approximation [22]. All of the introduced quantities vary along the z axis due to interaction in nonlinear media. The energy conversion efficiency to the sum frequency pulse is defined as $\eta_W(z) = W_3(z)/\left[W_1(z=0) + W_2(z=0)\right]$.

According to the method recommended by the International Standardization Organization (see [27] and references therein), for experimental measurement of propagation factors it is necessary to measure energy density distribution after the focusing lens in a number of planes perpendicular to the beam propagation direction. Then the time-integrated pulse-propagation factor $\overline{M^2(t)}$ is defined on the basis of the fitting procedure of theoretical parabola to the squares of radii that are measured (or calculated) using the second moments of the energy density distribution function [14]. For calculating the time-resolved pulse propagation factor at a given time moment $M^2(t)$, it suffices to know the distribution of the complex amplitude $E(r,t,z)$ in the $z$ plane [13–17]. In the case of axially-symmetric beams, the propagation factor may be expressed as follows [15–17]:

$$M^2(t) = \left\{ \int_0^\infty \left| \frac{\partial E(r,t,z)}{\partial r} \right|^2 r\,dr \cdot \int_0^\infty \left| E(r,t,z) \right|^2 r^3 dr \right. \tag{5}$$

$$\left. -\frac{1}{4} \left| \int_0^\infty r^2 \left[ \frac{\partial E(r,t,z)}{\partial r} E^*(r,t,z) - E(r,t,z) \frac{\partial E^*(r,t,z)}{\partial r} \right] dr \right|^2 \right\}^{1/2} \times$$

$$\times \frac{1}{\int_0^\infty |E(r,t,z)|^2 \, r\,dr}.$$

Within the paraxial optics approximation, the values of the factor at different time moments $M^2(t)$ are conserved when the pulse propagates through optical systems described by ABCD matrices. Of course, the temporal shape of the instantaneous pulse power $P(t)$ is also conserved. Therefore, in [15] we have suggested to define the power-weighted time-averaged pulse propagation factor

$$\langle M^2(t) \rangle = \int M^2(t) P(t)\,dt \Big/ \int P(t) dt, \tag{6}$$

as a quantity that conserves during pulse propagation through optical systems described by ABCD matrices and is convenient for numerical calculations. The factor $\langle M^2(t) \rangle$ should be distinguished from the factor $\overline{M^2(t)}$. Only quite recently it has been shown that the propagation factor of a general pulsed paraxial beam, evaluated by the

standard second-moment method from the distribution of integral energy density values, is also conserved during the propagation through optical systems characterized by ABCD-matrices [28]. However, the evaluation of the factor $\overline{M^2(t)}$ requires additional resources of CPU time for the calculation of the propagation of the pulse being studied after the focusing lens, necessary to find the integral energy density distribution and mean-square radii of the beam in different planes along the propagation direction. At the same time, for calculating the factor $\langle M^2(t)\rangle$, it is sufficient to know the distribution of the complex field amplitude in some plane behind the nonlinear optical system, for instance, simply in the output plane, thus, to find $\langle M^2(t)\rangle$ it is sufficient to calculate integrals (5) and (6). In general case, no relation between the factors $\langle M^2(t)\rangle$ and $\overline{M^2(t)}$ has been established. Our numerical calculations have demonstrated that the propagation factors usually only slightly differ, by no more than 5-10% [16, 17]. Therefore, to characterize the pulse quality, we shall use the factor $\langle M^2(t)\rangle$ whose evaluation is much simpler.

## 3 Formulation of the mathematical problem

Passing to the dimensionless variables as in [16], the system of equations similar to that utilized in [18] can be readily obtained:

$$\frac{\partial A_l}{\partial z} + a_l \frac{\partial A_l}{\partial t} + ib_l \frac{\partial^2 A_l}{\partial t^2} + \frac{ic_l}{r}\frac{\partial}{\partial r}\left(r\frac{\partial A_l}{\partial r}\right) = id_l\varphi_l + e_l A_l. \quad (7)$$

Here $A_l(r,t,z)$ are complex valued functions, $l$=1, 2, 3; $a_l$, $b_l$, $c_l$, $d_l$, and $e_l$ are real constants; $\varphi_l$ are nonlinear functions, depending on $A_1$, $A_2$ and $A_3$:

$$\varphi_1 = A_2^* A_3 e^{-i\kappa z}, \quad \varphi_2 = A_1^* A_3 e^{-i\kappa z}, \quad \varphi_3 = A_1 A_2 e^{i\kappa z}. \quad (8)$$

System (7) is to be solved in the area $Q = [0,R]\times[0,Z]\times[0,T] \subset \mathbb{R}\times\mathbb{R}\times\mathbb{R}$. The physical meanings of the values $R$, $Z$, and $T$ are the radius of the nonlinear crystal, its length and time limit of the simulation. We also specify the initial and boundary conditions for this system of equations. The initial condition is

$$A_l(r,t,z=0) \;=\; A_l^0 \cdot e^{-\frac{r^{2S}}{w_l^{2S}}} \cdot e^{-2ln2\cdot\frac{(t-t_l)^2}{\tau_l^2}}, \quad A_j^0 \in \mathbb{C}. \tag{9}$$

The functions $A_j(r,t,z)$ must also satisfy the following boundary conditions:

$$\frac{\partial A_l(r=0,t,z)}{\partial r} = 0, \tag{10}$$

$$A_l(r=R,t,z)=0, \quad A_l(r,t=0,z)=0, \quad A_l(r,t=T,z)=0. \tag{11}$$

## 4 Numerical method of the solution

The numerical solution of the presented system (7) is performed on a uniform grid. The algorithm begins with a known layer at $z=0$ and moves upward with some step $\Delta z$. Every next layer is calculated in two steps:

1. First we use finite-difference method to solve the initial equation system (7) without the first order derivative $\frac{\partial A_l}{\partial t}$:

$$\frac{\partial A_l}{\partial z} + ib_l\frac{\partial^2 A_l}{\partial t^2} + \frac{ic_l}{r}\frac{\partial}{\partial r}\left(r\frac{\partial A_l}{\partial r}\right) = id_l\varphi_l + e_l A_l, \quad l=1,2,3; \tag{12}$$

2. Then, using numerical results obtained from the previous step, we solve the remaining transport equations:

$$\frac{\partial A_l}{\partial z} + a_l\frac{\partial A_l}{\partial t} = 0, \quad l=1,2,3. \tag{13}$$

The numerical values obtained in the second step are further used as input values to the first step to calculate next layer along the $z$ axis.

### 4.1 Finite-difference scheme for the Schrödinger equations

This sections goes into deeper details describing the first step of the solution outlined above. First, let us introduce a uniform grid with the steps $\Delta r$, $\Delta t$ and $\Delta z$ in the area of investigation $Q$ and the following notations on this grid:

$$\Delta r = R/N_r, \quad r_i = i\Delta r, \quad i = 0 \dots N_r; \tag{14}$$
$$\Delta t = T/N_t, \quad t_l = j\Delta t; \quad j = 0 \dots N_t; \tag{15}$$

The solving procedure begins with the known grid values on the grid layer at grid points $z = 0$. Using these values we further compute the values at the layer $z = \Delta z$ and so on, layer by layer. Therefore, it is convenient to introduce the following notations for the grid functions on two subsequent layers:

$$p = p^{ij} = p^{ij}(z) = A_l(r_i, t_j, z), \tag{16}$$
$$p^e = p^{ij}, \text{ if } i + j \text{ is an even number}, \tag{17}$$
$$p^o = p^{ij}, \text{ if } i + j \text{ is an odd number}, \tag{18}$$
$$\hat{p} = \hat{p}^{ij} = p^{ij}(z + \Delta z), \tag{19}$$
$$p_{\bar{t}t} = \frac{p^{j+1} - 2p + p^{j-1}}{\Delta t^2}, \tag{20}$$
$$p_{\dot{r}r} = \frac{r_{i+\frac{1}{2}}(p^{i+1} - p) - r_{i-\frac{1}{2}}(p - p^{i-1})}{\Delta r^2}, \tag{21}$$
$$\varphi = \varphi^{ij} = \varphi_l\Big(A_1(r_i, t_j, z), A_2(r_i, t_j, z), A_3(r_i, t_j, z)\Big). \tag{22}$$

To decrease the number of indices used to define the difference scheme, further we use only the "neighbor" indices, i.e., we write $p^{i+1}$ and $p^{j-1}$ instead of $p^{i+1j}$ and $p^{ij-1}$. Writing the grid functions, we also omit the index $l$ because these functions are defined identically for every equation in the system (12).

Using the Hopscotch type scheme [29], we transform the differential equation system (12) into a set of difference equations by introducing an intermediate layer $\tilde{p} = \tilde{p}^{ij} = p^{ij}(z + \Delta z/2)$:

$$2\frac{\tilde{p}^e - p^e}{\Delta z} + ib_l p^e_{\dot{t}\dot{t}} + \frac{ic_l}{r} p^e_{\dot{r}r} = id_l\varphi^e + e_l p^e, \quad (23)$$

$$2\frac{\tilde{p}^o - p^o}{\Delta z} + ib_l \tilde{p}^o_{\dot{t}\dot{t}} + \frac{ic_l}{r} \tilde{p}^o_{\dot{r}r} = id_l\tilde{\varphi}^o + e_l \tilde{p}^o, \quad (24)$$

$$2\frac{\hat{p}^o - \tilde{p}^o}{\Delta z} + ib_l \tilde{p}^o_{\dot{t}\dot{t}} + \frac{ic_l}{r} \tilde{p}^o_{\dot{r}r} = id_l\tilde{\varphi}^o + e_l \tilde{p}^o, \quad (25)$$

$$2\frac{\hat{p}^e - \tilde{p}^e}{\Delta z} + ib_l \hat{p}^e_{\dot{t}\dot{t}} + \frac{ic_l}{r} \hat{p}^e_{\dot{r}r} = id_l\hat{\varphi}^e + e_l \hat{p}^e. \quad (26)$$

According this scheme, even and odd grid points are computed separately. First, using known values of $p$, the values at even grid points on the intermediate layer ($\tilde{p}^e$) are computed. This difference equation system (23) is explicit, since it uses only the known values on the previous layer $p$ and the grid function $\tilde{p}$ occurs only in linear expressions. After solving this system of equations, we know all the even values and the values on the border of the intermediate layer $\tilde{p}$.

The second difference equation system (24) defines the way the odd grid points $\tilde{p}^o$ are computed using odd points of the lower layer and already known even points of the intermediate layer. Here we have to solve the system of nonlinear equations with three variables, because the unknown variables occur in nonlinear expressions $\varphi$. We solve this system of equations using an iterative method.

The third and the fourth system of difference equations are used to compute grid points of the upper layer ($\hat{p}$). They are equivalent to the first ones with the exception to the order the grid points are computed: first the odd and then the even ones.

### 4.2 Approximation of the boundary conditions

To solve the systems of equations described in the previous section we need to use the boundary conditions. The approximation of the boundary value conditions (11) is straightforward. At the boundaries $r = R$, $t = 0$ and $t = T$ we assume that grid functions $p$ have zero values:

$$p^{N_r j} = 0, \quad j = 0 \dots N_t; \quad (27)$$

$$p^{i0} = 0, \quad i = 0 \dots N_r; \quad (28)$$

$$p^{iN_t} = 0, \quad i = 0 \dots N_r. \quad (29)$$

The remaining boundary condition (10) is approximated in two different ways depending on the parity of the grid points.

### 4.3 Solution of the transport equations

The remaining part of the simulation is the solution of transport equations (13). Usually this equation is solved by using the fast Fourier transform method [20, 21]. Transport equations only shift the already computed numerical values by $a_l \Delta z$. Thus we can simply interpolate those values at the grid points shifted by $a_l \Delta z$. This was carried out using the cubic spline interpolation method [30].

The finite-difference method described in the previous section possesses the following property: the even grid point values are computed separately from the odd grid point values. Thus the shapes of the resulting even and odd grid functions are always slightly different. These differences compensate one another, because we use the steps interchangeably. But now we added the interpolation between subsequent iterations of finite-difference calculations.

We observed that spline interpolation used after the whole iteration of finite-difference method (23-26) cause growth of the computation error. To keep this error low we use the spline interpolation after computing values for every new layer: both the intermediate (23-24) and the upper one (25-26). Thus we use finite-difference and spline interpolation methods interchangeably.

To apply the spline interpolation twice while computing the new upper layer, we have to use a smaller shift value: $a_l \Delta z/2$.

## 5 Results of numerical modeling of SHG

Numerical simulation of the second harmonic generation using ultrashort laser pulses with inter-pulse delay was performed for the conditions close to those described in [18], where the experimental research of SHG in a type II KDP crystal was carried out using the fundamental harmonic (FH) pulses of a neodymium-glass laser (wavelength $\lambda = 1053$ nm) with duration of 1 ps and intensity of up to 100 GW/cm$^2$. The values of the physical parameters of the KDP crystal required for the numerical simulation were taken from [7, 8, 18, 25]. The following normalization constants were used: $r_0 = 2$ cm, $t_0 = 1$ ps, $z_0 =$

$\nu_{1e}t_0 = 0.2019$ mm, where $\nu_{1e} = \nu_2$ is the group velocity of the fastest FH pulse with extraordinary polarization. The normalization value of the electrical field strength $E_0$ was chosen in such a way that the modulus of the complex amplitude $|A_2| = |E_2|/E_0 = 1$ for the fundamental harmonic with extraordinary polarization be equal to the intensity 100 GW/cm$^2$. Taking into account the fact that the refraction indices for the ordinary and extraordinary beams of the fundamental harmonic, as well as that for the extraordinary beam of the second harmonic, are of similar numerical magnitudes, $|A_l| = 0.1$ corresponds to 1 GW/cm$^2$ with a high accuracy. In order to simplify the graphical representation of the calculation results, the intensity as well as the power, the energy density and the total pulse energies expressed in terms of it in dimensionless units were denoted by the same symbols, and the intensity was assumed to be $I_l(r,t,z) = |A_l(r,t,z)|^2$.

To obtain the results presented below, it was assumed for simplicity that the linear phase matching condition was met ($\kappa = 0$) and that the walk-off effect could be neglected for broad ($w_1 = w_2 = 0.3$ in normalized dimensionless units) super-Gaussian ($S = 2$) beams. In order to exclude the effects of the cubic nonlinearity of the crystal, the calculations were performed for intensities lower by approximately an order of magnitude ($A_1 \cong A_2 \sim 0.3$) than those in [18]. The influence of the linear absorption was also neglected, since the KDP crystal is transparent for both the fundamental and the second harmonics of the Nd:glass laser. The delay between the FH pulses was controlled by the difference of the time moments $\Delta t = t_2 - t_1$ of the peak intensities of the pulses. To implement the pulse compression regime, the crystal length should be sufficient for the pulse with higher group velocity, delayed by a time of the order of the initial pulse duration, to overtake the pulse with lower group velocity during the propagation time in the crystal. The algorithm and program developed enable us to follow the pulse propagation in the crystal and thus to optimize the SHG process (for instance, in order to achieve a highly-efficient energy conversion and short pulse duration with acceptable quality degradation of the second harmonic pulses).

The calculation results presented below for the incoming pulses with the amplitudes on the beam axis $A_1^0 = A_2^0 = 0.3$, the duration $\tau_1 = \tau_2 = 1$ and the time delay $\Delta t = 0.7$ ($t_2 = 2.7$, $t_1 = 2.0$)

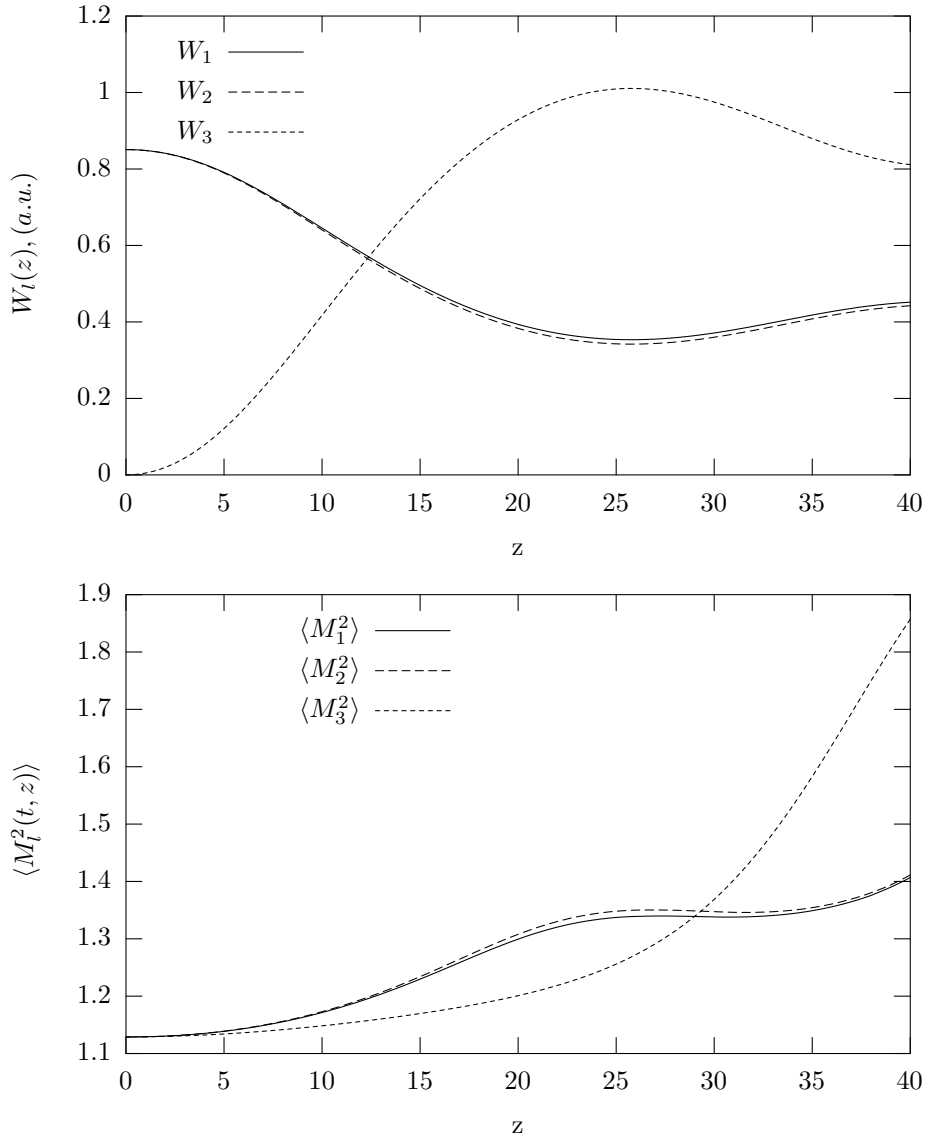


Figure 1: Energies and beam propagation factors of FH and SH pulses at different planes in the doubling crystal of type II with a time predelay

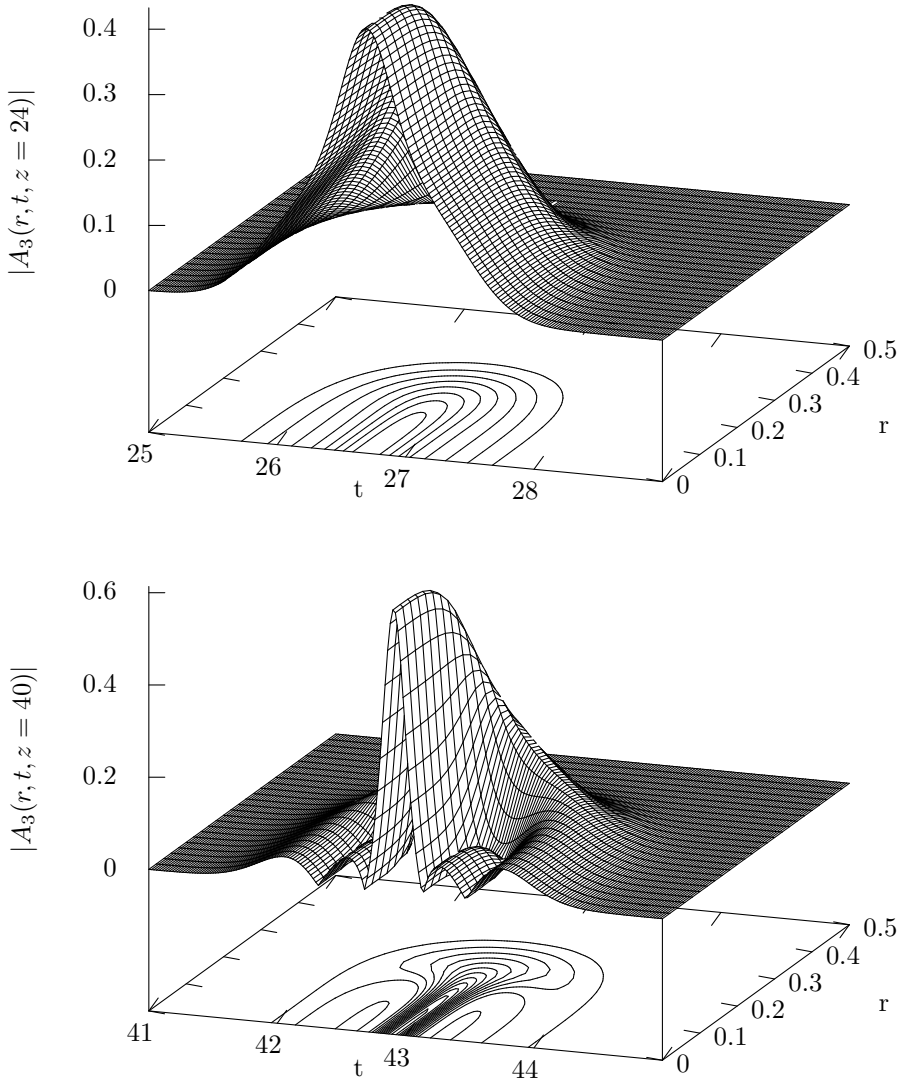


Figure 2: Spatial-temporal structure of SH pulses at the plane of maximum energy conversion (z=24) and at the crystal exit plane (z=40)

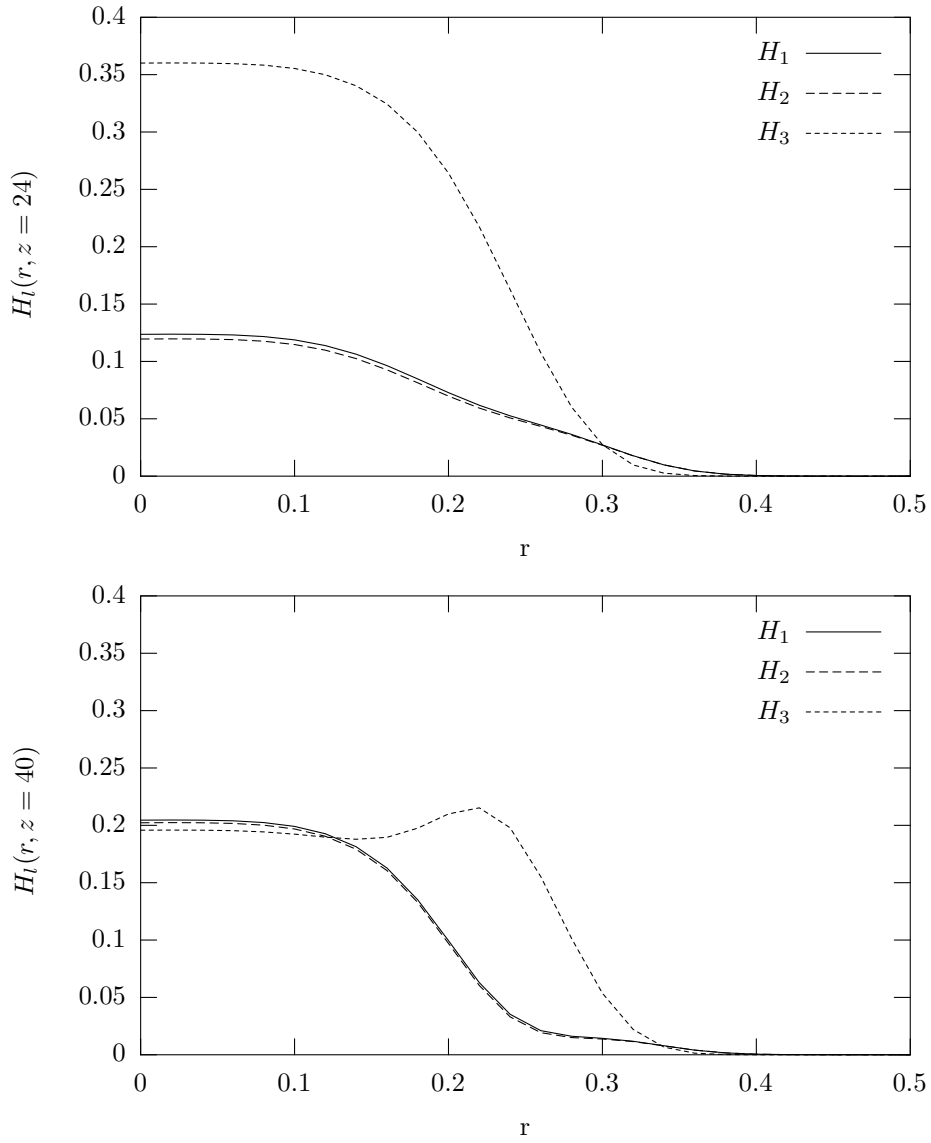


Figure 3: Transverse energy density distributions of FH and SH pulses at the plane of maximum energy conversion (z=24) and at the crystal exit plane (z=40)

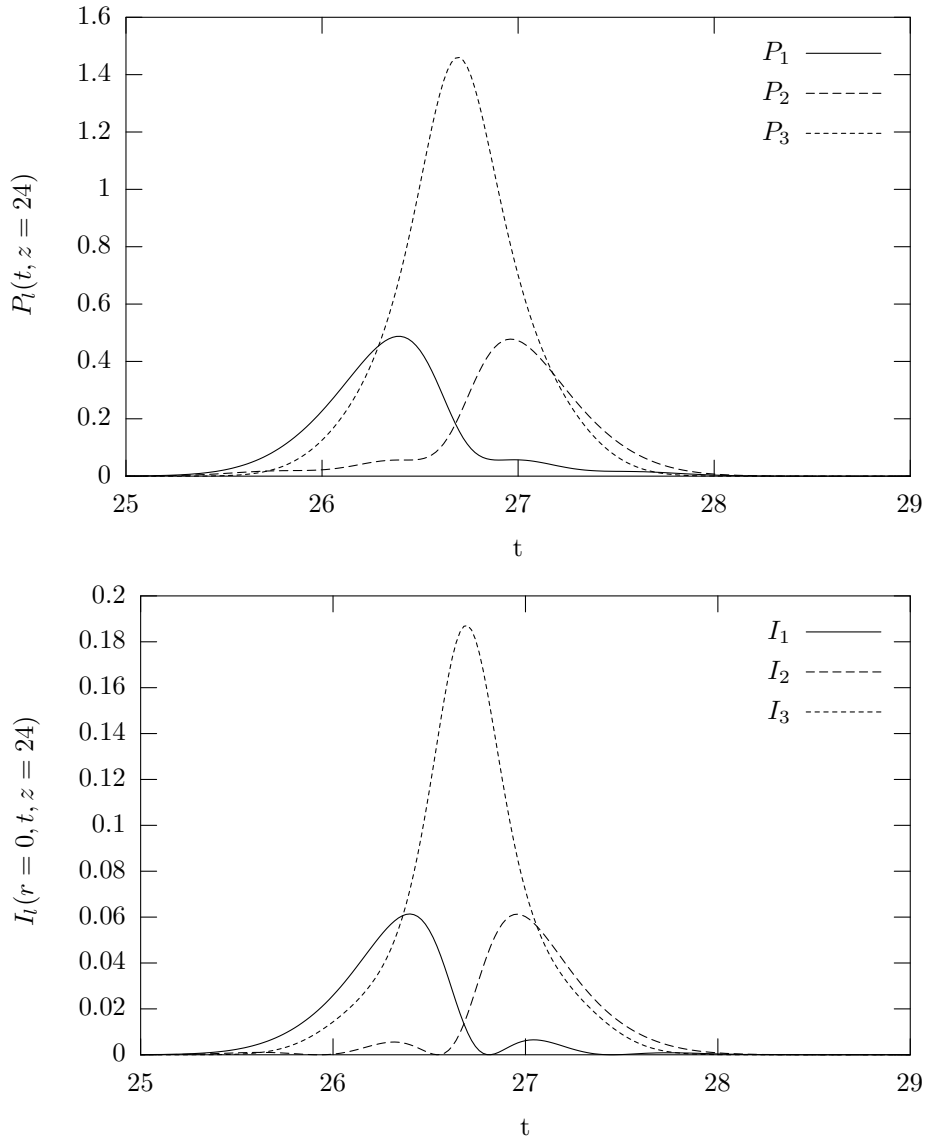


Figure 4: Temporal shapes of FH and SH pulse power and pulse intensity on the axis of beams at the plane of maximum energy conversion (z=24)

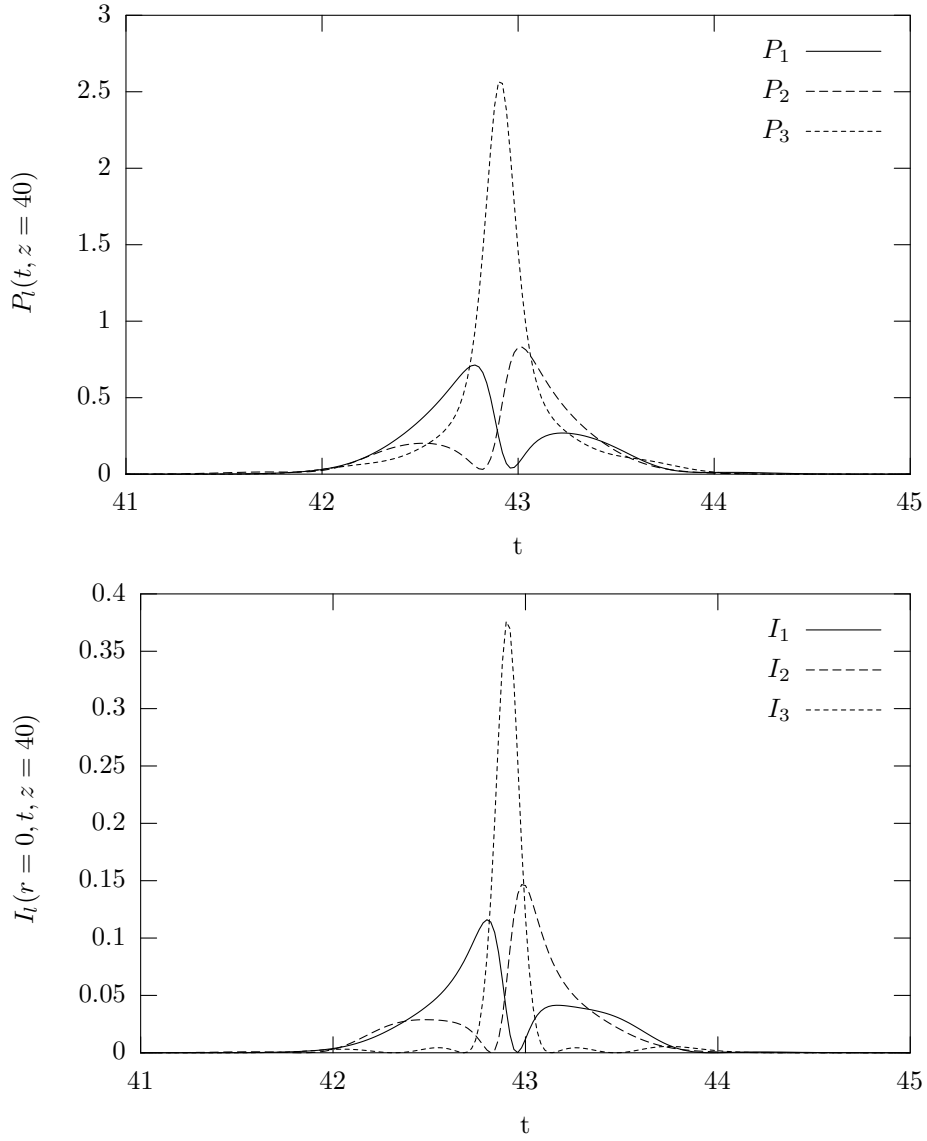


Figure 5: Temporal shapes of FH and SH pulse power and pulse intensity on the axis of beams at the crystal exit plane (z=40)

demonstrate that the maximum energy conversion to the second harmonic $\eta_W = 60\%$ at the indicated input intensities is achieved at the plane $z = 24$ (Fig. 1), where the pulse propagation factors of the fundamental and the second harmonic $\langle M_l^2(z = 24)\rangle$ only slightly exceed the propagation factor of the initial collimated super-Gaussian beams [16]. Results of simulation presented in Fig. 1 and other figures below were computed using the following steps: $\Delta r = 0.02$, $\Delta t = 0.02$ and $\Delta z = 0.02$. The calculations with these step values satisfy the energy conservation law with enough good accuracy ($< 1\%$). The spatio-temporal structure of the second harmonic pulses (Fig. 2), including the transverse energy density distribution in the interacting beams (Fig. 3), remain smooth. However, the compression rate of the second harmonic pulses in this case is only $N = \tau_1/\tau_3 \approx 2$ (Fig. 4). It should be noted that on the beam axis, i.e., basically in the plane wave approximation, the pulse is additionally compressed (at half the peak intensity level) to the duration $\tau_3^I = 0.46$, while the pulse duration at half the peak power is reduced significantly less ($\tau_3^P = 0.58$).

As the pulse further propagates in the crystal, the reverse energy transfer from the second harmonic pulse to the FH pulse begins (Fig. 1), during which the duration of the second harmonic pulse continues to decrease (Fig. 5). However, this results in rather significant distortion of the spatio-temporal structure of the second harmonic pulse (Fig. 2), rapid increase of the propagation factor $\langle M_l^2(z)\rangle$ that characterizes the beam quality $\langle K_l\rangle = 1/\langle M_l^2\rangle$, and formation of the ring-shaped transverse distribution of the energy density (Fig. 3). For most of the practical applications, sufficiently high beam quality is necessary. Assuming that the quality parameter $\langle K\rangle$ must exceed, say, 0.5, we can conclude that the crystal length for the set intensity of the incoming pulses should not exceed $L = 8$ mm ($z = 40$). In this case, duration of the compressed second harmonic pulses at the exit from the crystal is $\tau_3^P = 0.19$ by power and $\tau_3^I = 0.15$ by intensity (Fig. 5). Thus, during the process of the backward energy transfer, the duration of the second harmonic pulse decreases by a factor of three, while its energy decreases by only a factor of 1.25. Consequently, the intensity and the power increase twice in this case with acceptable quality degradation.

## 6 Conclusion

We describe simulations of the second harmonic generation of ultra short laser pulses by numerically solving a system of wave propagation equations. Equations are solved by using split-step method in two-dimensional cyllindrically symmetric space and time coordinates. The diffraction part of a solution uses Hopscotch type finite-difference scheme on a regular grid. The transport part is solved by using cubic spline approximation. The obtained numerical results satisfactorily respect energy conservation constraints.

The algorithm and the program developed makes it possible to optimize the process of the second harmonics generation and to identify the conditions where sufficiently high degree of the pulse compression with relatively low degradation of their quality is achieved.

Concrete calculations for the compression regime in the KDP crystal have demonstrated that the propagation factor $\langle M_3^2(t)\rangle$ describing the quality of the second harmonics pulse only slightly exceeds the propagation factor of the initial first harmonics pulses $\langle M_1^2(t)\rangle = \langle M_2^2(t)\rangle$ at the moment of the maximum energy conversion. However, it starts to increase quite rapidly during the backward energy transfer to the pulses of the first harmonics, during which significant shortening of the second harmonics pulses takes place.

## References


[1] Sutherland R.L. *Handbook of Nonlinear Optics.* Marcel Dekker Inc., New York, 1996.

[2] Wang Y., Dragila R. "Efficient conversion of picosecod laser pulses into second-harmonic frequency using group-velocity-dispersion". *Phys. Rev. A*, 41:5645, 1990.

[3] Stabinis A., Valiulis G. "Sum frequency pulse compression due to depletion of interacting waves". *Lasers and ultrafast processes*, 3:9, 1990.

[4] Stabinis A., Valiulis G., Ibragimov E.A. "Effective sum frequency pulse compression in nonlinear crystals". *Opt. Commun.*, 86:301, 1991.

[5] Wang Y., Luther-Davies B. "Frequency-doubling pulse compressor for picosecond high-power neodymium laser pulses". *Opt. Lett.*, 17:1459, 1992.

[6] Chien C.Y., Korn G., Coe J.S., Squier J., Mourou G., Craxton R.S. "Highly efficient second-harmonic generation of ultraintense Nd:glass laser pulses". *Opt. Lett.*, 20:353, 1995.

[7] Zhang T., Daido H., Kato Y., Sharma L.B., Izawa Y., Nakai S. "Second-harmonic generation of a picosecond laser pulse at a high intensities with time predelay". *Jpn. J. Appl. Phys.*, 34:3546, 1995.

[8] Zhang T., Kato Y., Yamakawa K., Daido H., Izawa Y. "Peak intensity enhancement and pulse compression of a picosecond laser pulse by frequency doubling with a predelay". *Jpn. J. Appl. Phys.*, 34:3552, 1995.

[9] Umbrasas A., Diels J-C., Jacob J., Valiulis G., Piskarskas A. "Generation of femtosecond pulses through second-harmonic compression of the output of a Nd:YAG laser". *Opt. Lett.*, 20:2228, 1995.

[10] Biegert J., Kubecek V., Diels J-C. "Pulse compression". In Webster J.G., editor, *Wiley Encyclopedia of Electrical and Electronics Engineering*, volume 17, page 446. John Wiley&Sons Inc., 1999.

[11] Zhang T., Kato Y., Daido H. "Efficient third-harmonic generation of a picosecond laser pulse with time delay". *IEEE J. Quant. Electron.*, 32:127, 1996.

[12] Dubietis A., Tamošauskas G., Varanavičius A. "Femtosecond third-harmonic pulse generation by mixing of pulses with different duration". *Opt. Commun.*, 186:211, 2000.

[13] Smith A.V., Bowers M.S. "Phase distortions in sum- and difference-frequency mixing in crystals". *J. Opt. Soc. Am. B.*, 12:49, 1995.

[14] Smith A.V., Alford W.J., Raymond T.D., Bowers M.S. "Comparison of a numerical model with measured performance of a seeded, nanosecond KTP optical parametric oscillator". *J. Opt. Soc. Am. B.*, 12:2253, 1995.

[15] Buzelis R., Vaicekauskas R., Dement'ev A., Ivanauskas F., Kosenko E., Murauskas E., Radžiūnas M. "Numerical analysis and experimental investigation of generation, SBS-compression and amplification of short Nd:YAG laser pulses". *Izv. RAN, Ser.Fiz.*, 60:169, 1996. In Russian.

[16] Buzelis R., Dement'ev A., Kosenko E., Murauskas E., Vaicekauskas R., Ivanauskas F. "Amplification efficiency and quality alteration of sort pulses amplified in the Nd:YAG amplifier in the saturation mode". *Lithuanian Phys. J.*, 38:289, 1998.

[17] Dement'ev A., Čiegis R., Ivanauskas F., Girdauskas V., Lasys V., Navakas R., Rate P., Vaicekauskas R., Vrublevskaya O. "Modelling of changes of pulse propagation factors in nonlinear optical processes". In H.Weber, H.Laabs, editor, *Laser Beam and Optics Characterization*, pages 238–259, Technische

Universität Berlin, Optisches Institut, Strasse des 17. Juni 135, D-10623 Berlin, Germany, 2000.

[18] Zhang T., Yonemura M. "Tranverse-mode effect of second-harmonic generation of ultrashort laser pulses with time delay". *Jpn. J. Appl. Phys.*, 37:5569, 1998.

[19] Zhang T., Yonemura M. "Pulse shaping of ultrashort laser pulses with nonlinear optical crystals". *Jpn. J. Appl. Phys.*, 38:6351, 1999.

[20] Vasiliauskas V., Ivanauskas F., Stabinis A. "Stationary parametric amplification of spreading light pulses under condition of group velicity mismatch". *Kvantovaya Elektronika*, 13:833, 1986. In Russian.

[21] Ivanauskas F., Stabinis A. "The method of total approximation for calculation of three-frequences interactions of electromagnetic waves in nonlinear medium". *Differential equations and their applications*, 38:23, 1986. In Russian.

[22] Karamzin Yu.N., Sukhorukov A.P., Trofimov V.F. *"Mathematical Modelling in Nonlinear Optics"*. Moscow University Press, 1989. In Russian.

[23] Dmitriev V.G., Tarasov L.V. *"Applied Nonlinear Optics"*. Radio and Communication, Moscow, 1982. In Russian.

[24] Banfi G.P. "Nonlinear propagation in homogeneous media". In *Nonlinear Optical Materials: Principles and Applications*, page 73. IOS Press, Amsterdam, 1995.

[25] Dmitriev V.G., Gurzadyan G.G., Nikogosyan D.N. *"Handbook of Nonlinear Optical Crystals"*. Springer, Berlin, 1997.

[26] Menza L. D. "Numerical simulation with finite differences of wave propagation in diffractive quadratic media". *J. Opt. B: Quantum Semiclass*, 1:19, 1999.

[27] Buzelis R., Dement'ev A., Vaicekauskas R., Ivanauskas F., Radavičius M. "Laser beam quality parameter measurement using CCD cameras". *Lithuanian Phys. J.*, 38:159–164, 1998.

[28] Cao Q., Deng X. "Spatial parametric characterization of general polychromatic beams". *Opt. Commun.*, 142:135–145, 1997.

[29] Radžiūnas M., Ivanauskas F. "The stability conditions of finite difference schemes for Schrödinger, Kuramoto-Tsuzuki and heat equations". *Math. Modeling and Analysis*, 3:177–194, 1998.

[30] William H. Press, Saul A. Teukolsky, William T. Vetterling, Brian P. Flannery. *Numerical Recipes in C: The Art of Scientific Computing*, pages 113–116. Cambridge University Press, second edition, 1993.